ChemPubSoc Europe

DOI: 10.1002/ejic.201501342

EurJIC European Journal of Inorganic Chemistry

Microreview

Electron Microscopy

What Can Electron Microscopy Tell Us Beyond Crystal Structures?

Wuzong Zhou*[a] and Heather F. Greer[a]

Abstract: Transmission electron microscopy is a powerful tool to directly image crystal structures. Not only that, it is often used to reveal crystal size and morphology, crystal orientation, crystal defects, surface structures, superstructures, etc. However, due to the 2D nature of TEM images, it is easy to make mistakes when we try to recover a 3D structure from them. Scanning electron microscopy is able to provide information on the particle size, morphology and surface topography. However, obtaining information on crystallinity of particles using SEM is difficult. In this microreview article, some practical cases of transmission and scanning electron microscopy investigations of inorganic crystals are reviewed. Commonly occurring uncertainties, imperfection and misunderstandings are discussed.

1. Introduction

Although electron microscopy related techniques, such as transmission electron microscopic (TEM) imaging, high resolution TEM (HRTEM) imaging, selected area electron diffraction (SAED), and energy dispersive X-ray microanalysis (EDX), can reveal crystal structures, X-ray and neutron diffraction methods are much more accurate in determination of average crystal structures.[1] Nevertheless, electron microscopy techniques are often used to complement powder X-ray diffraction data (PXRD) to solve complex crystal structures.[2] Although collection of a PXRD pattern is easy, the data can often be difficult to interpret due to a phase problem, broadening or overlap of reflections with similar diffraction angles, especially when the structure has a large unit cell or low symmetry. Typically, in order to determine a complex structure, PXRD intensity data is combined with structure factor phase information from HRTEM images,[3] rotation electron diffraction (RED)[4] or precession electron diffraction (PED).[2,5]

The most significant characteristic of electron microscopy is that it can directly show local structures in an atomic scale or a nanometer scale.[6] For nanomaterials, e.g. nanoparticle catalysts, nanowires and nanotubes of metal oxides, HRTEM is particularly useful, since the dimensions of the nanomaterials are often too small to give sufficient structural information in conventional diffraction experiments, such as X-ray diffraction (XRD) and neutron diffraction.[7] HRTEM images of thick samples often present complicated contrast patterns, which are not simply dependent on the crystal structures, due to multiple scattering of the electron beams. Computer simulation is the

[a] *School of Chemistry,*
University of St Andrews
St Andrews KY16 9ST, United Kingdom
E-mail: wzhou@st-andrews.ac.uk
http://www.st-andrews.ac.uk/chemistry/contact/academic/#wzhou

Wuzong Zhou is Professor of Chemistry at the University of St Andrews. He obtained his BSc in 1982 (Fudan University) and PhD in 1988 (University of Cambridge). His interests are in solid state chemistry in general, HRTEM investigations of defects in solids and non-classical mechanisms of crystal growth.

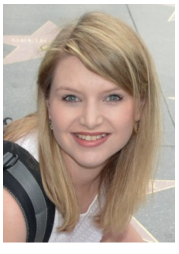

Heather F Greer is a Research Fellow at the University of St Andrews. She received her B.Sc in Chemistry and Mathematics at the University of St Andrews in 2009, and her PhD there in 2013. Her current research interests are the electron microscopic investigation of early stage crystal growth and reversed crystal growth of various solid state materials.

common trial and error method to assess the proposed structural models. For nanomaterials, on the other hand, this multiple scattering effect can be ignored, and the explanation of the HRTEM images is relatively simple. In many cases, determination of average crystal structures of bulk materials is often not enough for us to understand the physico-chemical properties. When individual particles are examined using electron microscopy, much more information beyond average crystal structures can be obtained, including particle size and shape, crystal orientation, defects, crystallinity, surface structures, superstructures, etc.[8] These microstructures play important roles in exhibiting material properties. However, the explanations of the experimental data are not always straightforward.

In this microreview, some practical cases of electron microscopic investigations of inorganic crystals are discussed. Common misunderstandings are explained and rectified, and the limits of the techniques are clearly delineated.

2. Crystal Size and Morphology

Among all the extra structural features detectable by electron microscopy, the easiest target is to determine crystal size and morphology. Particle size of a powder sample can be directly observed from TEM and SEM images. However, the inherent disadvantage of electron microscopy is that the number of particles examined is always limited. When we have recorded a TEM/SEM image of particles, a common question for ourselves is that whether this image is typical for the sample. To convince ourselves, we normally check the sample preparation method for TEM and make sure that the particles deposited on a specimen grid is not size selective. We also observe and record a large number of particles, at both low and high magnifications although only one or two images may be used in a final presentation. This will increase the likelihood of an impartial representation of the sample, although this can be quite time consuming and expensive. When the number of measured particle sizes is large enough (say 300 to 500), the size distribution should show a smooth log-normal distribution curve.[9]

With advances in synthesis capabilities the size of nanoparticles is steadily decreasing and moving towards a level where nanoparticles can consist from a small, predetermined number of atoms.[10] This leaves an even greater demand for accurate nanoparticle size distribution analysis. TEM, out of all the existing experimental techniques capable of measuring the particle size, is one of few techniques that allows direct (real space) visualisation of the nanoparticles. Using electron tomography, 3-dimensional images of nanoparticles can be shown. Pyrz and Buttrey[10] outlined a selection of topics which should be considered to avoid over-interpretation or the improper use of the information provided in TEM micrographs in regards to particle size characterisation. The issues include magnification, analysis method (manual vs. automated) and imaging type, (bright vs. dark field) and (TEM vs. STEM). Comparison of size measurements of nanoparticles > 5 nm in diameter by HRTEM and annular dark field scanning transmission electron microscopy (ADF-STEM) have been reported to agree very well. In contrast, similar measurements for smaller particles (<2 nm) were found to significantly differ. HRTEM has been said to overlook some particles, <2 nm in diameter, if they are amorphous or oriented off Bragg conditions.[11] It should also be noted that electron beam damage of the sample can cause modifications in the particle size, composition and/or morphology due to particle destruction/decomposition or particle coalescence.[12,13]

For nanoparticles, the crystal sizes can also be calculated from the Scherrer equation based on measuring XRD peak width at half the maximum intensity after subtraction of the background:

$$\tau = \frac{k\lambda}{\beta\cos\theta}$$

where τ is the mean size of the crystalline domains, k is a shape factor, λ is the X-ray wavelength, β is the line broadening at half the maximum intensity (FWHM) in radians, θ is the Bragg angle. Instrumental factors which affect peak width must be taken into account. The upper size limit for crystallite size measured using the Scherrer equation is an open question but is thought to be about 100–200 nm.[14] However, particle sizes obtained from electron microscopy and the crystallite size from XRD are often in disagreement, especially those with crystallites larger than 50–60 nm or with anisotropic morphologies.[15] If the particle size is small, e.g. < 10 nm in diameter, with a narrow distribution, and all particles are highly likely to be single crystals, the average particle sizes measured from TEM images and calculated from XRD patterns often are in good agreement. On the other hand, the calculated size from XRD can be much smaller than that directly observed from TEM images. The main reasons are that the detected dimensions of particles using these two techniques are not along the same orientation and that the terms, "particle size" and "crystal size" are two different concepts.

If the crystals have lamellar (nanosheet, plate or belt-like), nanoneedle, nanorod or nanowire morphology, crystallite size calculated from XRD is often a good estimate for the thickness/diameter of the crystallites but does not provide any indication of their length.[15] Revealing the dimension along the long axis of particles is much easier than observing the dimension along the short axis in TEM. For particles with anisotropic morphologies such as the above, the Scherrer size should only be stated with caution and displayed with complementary microscopic imaging data. In further instances where a sample contains "large" crystals of several microns and "small" crystals, say about 150–250 nm, the calculation of crystallite size via XRD would detect the presence of the small crystals but subsequently ignore the larger crystals.[15]

Another explanation for discrepancies in the crystallite size values from TEM and XRD is based on a factor that the particles are probably not single crystals. They may be polycrystalline or clusters of many smaller nanocrystallites.[16] They may also be hollow crystals, or crystals containing many defects or have incorporated organic matrix.[17,18] All types of crystal imperfections would lead to extra XRD peak broadening due to microstrain, resulting in a smaller value of crystal size.

Figure 1. (a) is a TEM image of part of a fish-bone like particle with many Co particles of different sizes located at the ends

of Mg_2SiO_4 nanorods. Sizes of the Co particles can be directly measured from this image. However, we are unable to tell whether these particles are single crystals until HRTEM images are obtained, although according to the classical crystal growth mechanism, the Co particles should grow up with layer-by-layer deposition of Co atoms and should be single crystals at any stage. HRTEM images of Co particles with different sizes revealed a non-classical growth route. The Co atoms deposit on the surface of Mg_2SiO_4 nanorods and combine into crystallites of 2 nm in diameter. These nanocrystallites do not undergo further growth, but aggregate into spherical polycrystalline clusters as shown in Figure 1 (b). Therefore, this particle has a particle size of about 30 nm in diameter as seen in the TEM image, but a crystal size of about 2 nm in diameter detectable by XRD. Only when the clusters approach to a certain size, they re-crystallize into single crystals, which often have a polyhedral shape (Figure 1, c).[19] Here we see that HRTEM images can show crystal fringes, and therefore the exact size of individual crystallites. Unfortunately the number of the crystallites examined by HRTEM is typically small.

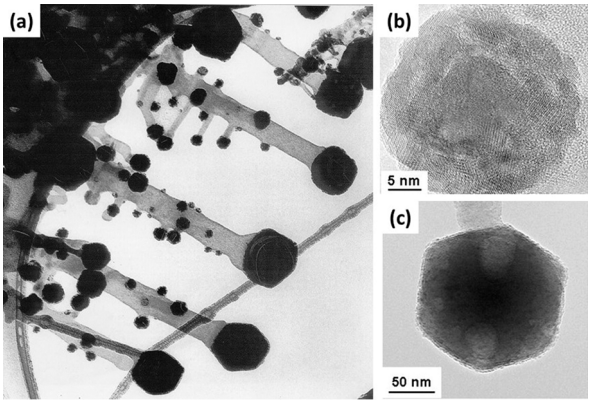

Figure 1. (a) TEM image of part of a fishbone-like particle showing lollipop-like secondary branches and sub secondary branches of Mg_2SiO_4 with Co particles at the ends. (b) HRTEM image of a Co particle of about 30 nm in diameter showing polycrystalline property. (c) TEM image of a Co single crystal, ≈ 150 nm in size, showing a polyhedral shape. [Reprinted with permission from *J. Phys. Chem.* **2004**, *B108*, 11561–11566. Copyright (2004) American Chemical Society].

SEM is a suitable technique to show particle morphologies. However, determining morphology of particles by TEM is not straightforward, since TEM only shows two dimensional projected images of three dimensional particles. For example, a cubic Co crystal could show a square shape when viewed down the <001> zone axes, or a rectangular shape along the <110> directions, or a hexagonal shape along the <111> directions (Figure 1, c). To reveal the actual shape of a particle, tilting the specimen grid to observe several projected images would be necessary. Determining crystal morphology using electron diffraction is also difficult, but not impossible, since the diffraction pattern can be affected by shape factors when the crystal size is small.[20] Using XRD or neutron diffraction method to determine crystal morphology is even more difficult.

Electron tomography is often an effective method used to reconstruct the 3D structure of nanoparticles from a single axis tilt series, typically +75° to –75°, of 2D STEM or TEM images.[21] Although this method can provide a real 3D representation of the crystal morphology, disadvantages include the difficulty to align the projections of a tomography tilt to a common axis with atomic precision and a "missing wedge" due to the inability to tilt ±90°.[22] Accuracy of the final reconstruction of the 3D volume relies on input from the number of projection images and tilt range but care should be taken to avoid electron beam damage or structural defomation during acquisition.

3. Crystal Facets and Growth Orientation

Many crystals appear as polyhedra with well defined facets. These polyhedra can be easily revealed from SEM images, which often give a 3D impression with significant image contrasts from different facets. However, to determine the crystal orientations of the facets from SEM images is not always achievable, unless electron backscatter diffraction (EBSD) is performed.[23] A perfect cubic particle can only be formed with six equivalent {100} facets of a crystal with a cubic structure. But a hexagonal morphology of a crystal with a hexagonal structure can be formed with two {001} and six {100} facets or six {110} facets. SEM images cannot be used to distinguish between them.

On the other hand, if particle size is very small, it is difficult to see the particle morphology in SEM images due to a resolution limit. TEM images are often used instead. However, the 2D nature of TEM images makes it difficult to recognise polyhedra. For example, a cubic Co crystallite can appear with a square shape in TEM images when the electron beam is parallel to the [001] zone axis. In this case, the observed four edges of the square particle correspond to the (100), ($\bar{1}$00), (010) and (0$\bar{1}$0) facets (Figure 2, a). SAED patterns can be used to confirm it. When the dimensions along the [100] and [010] axes are slightly different, a rectangular shape will be recorded in the TEM image. When viewing down the [110] direction of a cubic crystal, a rectangular shape is also observed in the TEM image as a projection of the particle. The crystal orientations of the 4

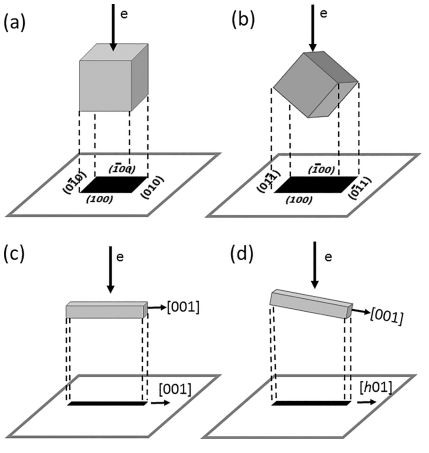

Figure 2. Schematic drawings of the relation between crystal orientations and projected shapes in TEM images. (a) Square shape on a TEM image as a result of projection of a cubic crystal along the [001] zone axis. (b) A rectangular shape on a TEM image when the view direction changes to [110]. (c) and (d) Projected TEM images of a nanorod with its long axis, the [001] zone axis, perpendicular and not perpendicular to the electron beam.

edges can be determined by the corresponding SAED patterns and HRTEM images to be [100], [$\bar{1}$00], [01$\bar{1}$] and [0$\bar{1}$1] (Figure 2, b). We can see that, in this case, the smooth edges of (01$\bar{1}$) and (0$\bar{1}$1) on the image of the particle do not mean there are such two facets. To understand what facets are present in TEM studies, we need to tilt the crystal to reveal its 3D morphology or to use SEM images as a reference to find out whether the observed crystal edges in TEM images correspond to crystal facets.[21] Consequently, the observed lattice fringes in a HRTEM image and the corresponding electron diffraction spots only indicate a crystal orientation which is perpendicular to the electron beam. It does not have a certain relation with a crystal facet. In other words, attempting to derive crystal facets merely from observed lattice fringes in HRTEM images or diffraction spots in SAED patterns is quite risky.

A similar confusion exists in TEM investigations of a crystal growth direction. Determination of the crystal growth direction is an important topic in the characterisation of low dimensional nanomaterials, and can have a large impact on understanding the physical and chemical properties of these materials.[24] For example, when nanorods or nanowires of a target material are fabricated, we wish to know what the crystal orientation is along the long axis, i.e. the prioritized growth orientation. When a nanorod with the growth direction along the [001] axis is examined in TEM, the growth direction can be determined by SAED or HRTEM imaging, subject to a correct position of the specimen.[25] Unfortunately in many studies, the growth direction of individual nanorods or nanowires is based on a single electron diffraction pattern or HRTEM image, leaving some degree of uncertainty. If the nanorod lies down on specimen grid with its long axis perpendicular to the electron beam, the diffraction spots along the growth direction in the SAED pattern and the corresponding lattice fringes on the HRTEM image would show the [001] orientation (Figure 2, c). However, if the nanorod is not perpendicular to the beam, the observed crystal orientation along the long axis of the projected nanorod image would be off the [001] zone axis, say for example the [h01] axis as shown in Figure 2 (d). The real growth orientation cannot be correctly revealed. It is difficult to distinguish these two cases from a single TEM image. Zou and co-workers also discussed this problem recently.[25] Rotation of the nanorod around the axis perpendicular to both the electron beam and the long axis of the nanorod allows us to find the position with the longest projected dimension of the nanorod image, at which the observed crystal orientation along the long axis and the real growth orientation are parallel to each other. A correct determination of the growth orientation is an important step prior to the design and growth of nanomaterials with desired orientations and properties. Changes in growth direction of nanowires are well known to affect their properties.[26]

4. Local Chemical Composition

Another advantage of electron microscopy is that the chemical composition of individual particles and even small areas, spanning several nanometers, in a particle can be analysed by EDX, since a very small beam size can be used. Variations of composition in a specimen can be examined using EDX point analysis and the elemental distribution in a particle can be shown in elemental mapping and electron energy loss spectroscopy (EELS).[27,28] For example, in a series of solid solution samples, EDX is normally used to confirm their homogeneity with different compositions.[29] It should be noted that, to determine an accurate chemical composition using EDX is not an easy job. This is because the intensity of an X-ray peak from an element is affected by many factors associated with a non-linear absorption problem, such as local composition, sample thickness, energy of electron beam, location of the sample area examined and its surrounding environment.[30] Therefore, in practice, in addition to keeping the same experimental conditions as much as possible, many spectra, e.g. from 20 to 30 randomly selected particles, should be collected in order to reduce the systematic error. During quantification a large source of error results from the overlap of peaks from different elements. For example, barium peaks overlap with titanium peaks, resulting in difficulties in the EDX analysis. The Ba Lα line appears at 4.4663 keV, whereas the Ti *K*α line occurs at 4.5089 keV. A correct identification often relies on recognizing peaks associated with each X-ray family. Furthermore, a suitable standard specimen with a pre-determined composition close to the target samples should be used to calibrate the results. For example, monophasic $BiNbO_4$ sample was used as the standard reference for an EDX study of solid solution in the Bi_2O_3-Nb_2O_5 system.[29]

Linear analysis and elemental mapping can supply information of elemental distribution and compositional variation in an examined specimen area.[31] For example, in a synthesized STA-7 zeolite sample, EDX point analysis indicated that the Si/Al ratio varies against the distance from the center to the edge of the crystals.[32] For some core-shell structures, the core and shell may have a similar structure and the HRTEM image contrast is not high, making it difficult to distinguish them. EDX elemental mapping, on the other hand, can show clearly the separation of compositions between the core and the shell in a nanometer scale.[27,33] In these studies, the accuracy of the chemical composition would not be high, but the inhomogeneous distribution of elements is obvious.

Elemental analysis using STEM has a tremendous advantage. STEM significantly reduces the interaction between the electron beam and the sample, therefore greatly reduces sample damage. It is noted that the recently developed state-of-the-art EDX system in a Cs corrected STEM can present elemental mapping at atomic resolution. However, the data can only be interpreted qualitatively because the elastic and thermal scattering of the electron probe confounds quantitative analysis.[34] High resolution elemental mapping can be collected with sample tilting to create a three dimensional re-construction. This method is particularly useful for particles with a domain structure, or core-shell structure, or any phase separation.

5. Surface Profile Imaging

Although elemental mapping is preferred for examination of chemical distribution in solids, narrow beam EDX technique is also used to detect the chemical composition of surface coating

nano-thick layers in crystals, when HRTEM surface profile images are observed.[35] HRTEM surface profile imaging is complementary to the standard surface science techniques such as scanning tunnelling microscopy (STM), atomic force microscopy (AFM), etc. The major difference is that STM and AFM show 2D images of the top surface layer, while HRTEM only shows 1D images of the top surface layer, i.e. a profile view.[36] However, this characteristic engenders an advantage of HRTEM: not only can the top surface be observed, but also the crystal structures underneath the surface can be imaged.[37] If the surface has a different crystalline phase, the thickness of this layer and its intergrowth with the core crystal can be revealed. For example, the (001) surface of La_2CuO_4 often terminates with several atomic layers of La_2O_3.[38] Regarding physico-chemical properties of inorganic solids, surface layers with nanometer scaled thickness is probably more important than only a top atomic layer. This advantage also makes HRTEM a suitable tool to investigate crystals with an amorphous surface coating layer.[39]

The amorphous layer on a crystal surface observed in HRTEM images could be due to decomposition of the parent crystal or deposition of amorphous carbon or other contaminates. The latter could form during synthesis or be deposited under electron beam irradiation. When both decomposed crystal and deposited amorphous carbon are present on crystal surface, their different image contrasts allow us to easily recognise them. The inner layer is normally the decomposed layer and the outer layer is contaminate. If there is only one amorphous layer, it is often difficult to determine whether it is decomposed crystal or deposited carbon. Making a conclusion without further testing would be inappropriate. An experienced operator would perform one or more experiments to discover the nature of a surface amorphous layer, if it is necessary.

First, if the coating layer is thick, e.g. a few nanomaters, using a narrow beam, the local chemical composition of the coating layer can be detected. A good example was demonstrated by EDX point analysis of an amorphous surface layer of Hg-containing high Tc superconducting cuprate. It was found that the surface of $HgBa_2CuO_4$ crystals often decomposed into an amorphous layer and lost Hg simultaneously.[40] Secondly, if an amorphous carbon layer formed during electron beam irradiation, its thickness may increase on extending the exposure time of electron beam as the hydrocarbon molecules are polymerised by the incoming (or outgoing) electrons.[13]

If the surface layer is decomposed crystal with the same composition as that of the parent crystal, it may recrystallize into the parent crystal under electron beam annealing. A clean crystal surface may be achieved as shown in HRTEM surface profile images of $YBa_2Cu_3O_7$.[41] Under electron beam irradiation, re-crystallisation started at the interface between the crystal and the amorphous layer, and extended across the whole amorphous layer. Finally, a clean surface is created (Figure 3). this work indicated that the decomposed surface of this specimen can be repaired by thermal annealing and can actually help to improve the quality of the superconducting property of the material. The decomposed layer on the surface of $HgBa_2CuO_4$ suffers a great loss of Hg, and therefore can only re-crystallise into barium copper oxide, which has a close relation in structure with $HgBa_2CuO_4$, and therefore, can intergrow with the parent crystal very well.[42]

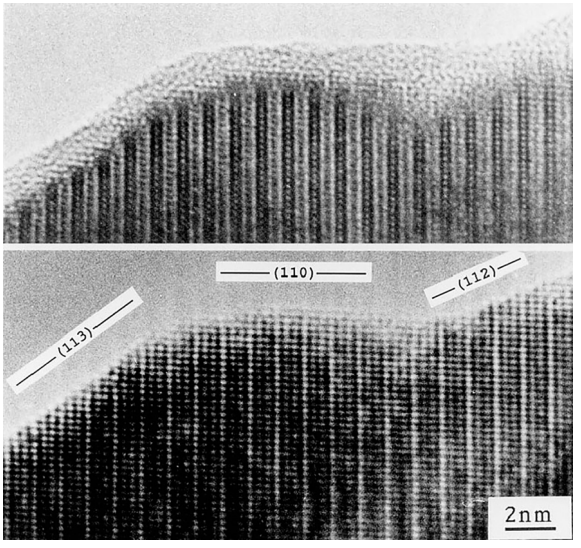

Figure 3. HRTEM surface profile images of $YBa_2Cu_3O_7$ viewed down the [110] direction. Top: the initial image showing a thin layer of disordered coating. Bottom: an image of the same area after electron beam irradiation for 3 hours. Clean (113), (110) and (112) surfaces are indicated. [Reprinted with permission from *J. Solid State Chem.* **1992**, *98*, 437–441. Copyright (1992) Elsevier Inc.].

Another example is that by Cölfen and co-workers[43] when they reported for the first time, a 3 to 5 nm thick continuous layer of amorphous calcium carbonate (ACC) on the surface of crystalline aragonite platelets in nacre of haliotis laevigata, a species of sea snail. Under intense electron irradiation, HRTEM images showed the ACC layer began to crystallise, forming several crystalline nuclei of aragonite that was slightly distorted compared with the core of the aragonite platelet.

6. Superstructures

Many superstructures in inorganic crystals occur due to ordering of lattice distortion or light elements. The scattering factor of electron diffraction, f_B, is very roughly proportional to $Z^{1/3}$ (Z: atomic number), while this order for X-ray scattering factor is about 1. This means that the scattering of electrons is less sensitive to atomic number. In other words, electron diffraction is a better method than XRD in detecting light elements, e.g. oxygen in metal oxides and, therefore, superstructures based on oxygen ordering.[7,44] In many cases, long-range ordering in complex solids such as $LiNi_{0.5}Mn_{0.5}O_2$ discovered by electron diffraction would be extremely difficult, if not impossible to detect by powder XRD and neutron diffraction.[45]

In Bi_2O_3-based solid solutions with guest oxides, Nb_2O_5, Ta_2O_5, V_2O_5, WO_3, several types of superstructures form with different compositions and can be revealed by SAED patterns and HRTEM images, although XRD patterns only show the fluorite basic sub-unit cells.[29,46] If it is a commensurate superstructure, the relation between the super unit cell and the basic unit cell is simple and can be described by a mathematical matrix. All the diffraction spots can be indexed to the superstructure.

When the positions of the diffraction spots were measured carefully, it was found that many superstructures in solid solutions were incommensurate.[47] Figure 4 shows some SAED patterns from some solid solution materials in the Bi-W-Nb-O mixed oxide system, along the [1$\bar{1}$0] zone axis of the fluorite subunit cell. The first impression might be that a threefold superstructure exists in these solids. A careful measurement, however, reveals that a true threefold superstructure only presents in $Bi_{10}W_2O_{21}$. In the other three SAED patterns, the two satellite diffraction spots due to the superlattice are not at the 1/3 and 2/3 positions in between (000) and (111) spots. An incommensurate structure can be regarded as a partially ordered structure, although unearthing a unit cell in a long range is impossible. On the other hand, to investigate the nature of the ordering, we can still focus on a small area in HRTEM images, from which a hypothetical commensurate super unit cell can be derived as a reasonable approach.[29]

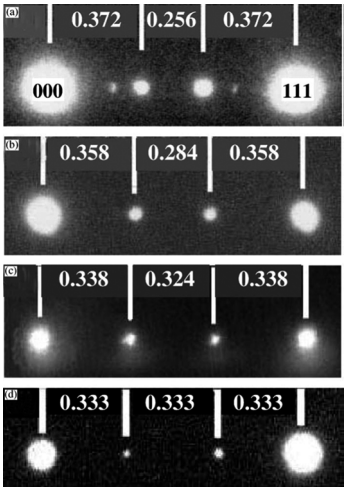

Figure 4. SAED spots along the [1$\bar{1}$0] direction of the fluorite-like subcell of some solid solution oxides in the Bi-W-Nb-O system, with compositions of (a) $Bi_8Nb_2O_{17}$, (b) $Bi_{17}WNb_3O_{36}$, (c) $Bi_{17}W_2Nb_3O_{39}$, and (d) $Bi_{10}W_2O_{21}$. The relative positions of the superstructure diffraction spots are indicated. [Reprinted with permission from *J. Solid State Chem.* **2002**, *163*, 479–483. Copyright (2002) Elsevier Science (USA)].

There is another reason to have extra weak diffraction spots in SAED patterns. Some systematically absent diffraction spots appear, which do not change the unit cell, but seem to reduce the symmetry of the structure. Possible multiple scattering effect should be considered. If this is the case, these extra diffraction peaks should not be observed in the corresponding XRD pattern, since no multiple scattering takes place in XRD. When the same SAED pattern is recorded at several areas with different specimen thickness, the relative intensities of these extra spots would be significantly changed. Specimen tilting would also notably change the relative intensities of the extra spots.

7. Defects

Investigation of defects in solids using electron microscopy is a common and important research field. The defects, including point defects, layered defects, twin defects, anti-phase defects, stacking faults, domain structures, dislocations[48] etc., can significantly affect the properties of the materials. In this article, electron microscopic images of some not obvious or hidden defects are discussed.

7.1. Twin and anti-Phase Defects

Both twin defects and anti-phase defects have a planar boundary and have two domains with identical crystal structures. When viewing down a direction parallel to an anti-phase boundary plane and perpendicular to the vector of phase shifting, the HRTEM image would show a dark contrast line on the boundary and, on the two sides of the boundary, the lattice patterns would shift to each other by a dimension of half a unit cell.[49] The dark image contrast is mainly contributed from diffraction contrast. In low magnification TEM images, no lattice fringes can be observed, but the image contrast of the anti-phase boundary is higher. This contrast can be even further enhanced by using a smaller objective aperture.

In the case of a twin defect, a dark line on the twin boundary can also be observed when the electron beam is parallel to the twin plane. The lattice patterns on both sides have mirror symmetry with the principal crystal orientation which bends to an angle smaller than 180°. Figure 5(a) shows a HRTEM image of a Si nanowire containing two twin defects, when viewed down the [11$\bar{1}$] zone axis. When the nanowire was rotated around the long axis of the nanowire by a small angle (e.g. 15°), the mirror symmetric lattice patterns disappeared and the fine dark lines of the twin planes became less obvious. A more fascinating change is that the lattice fringes may extend across the twin boundaries (Figure 5, b). This experiment tells us that a 2D planar defect boundary can unquestionably only be observed when viewing down the correct direction. A HRTEM image like that in Figure 5(b) does not mean it is defect free. The twin planes are actually hidden at the positions of wide dark belt-shaped regions, resulting from a projection of the twin planes with a tilted angle.[50] For the same reason, in a profile HRTEM image of a cyclic twinning nanowire containing five twin planes in a fivefold symmetry, no more than one twin plane can be observed at the same time.[20]

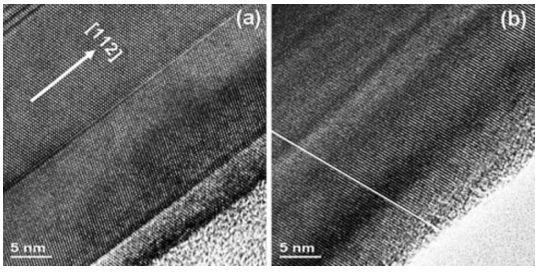

Figure 5. (a) HRTEM image of a Si nanowire with two twin defects. (b) HRTEM image of the same nanowire after rotating about 15° around the [112] axis. The straight line indicates the lattice fringes extend across the original twin defect planes. [Reproduced from ref. [50] with permission from The Royal Society of Chemistry].

7.2. Point Defects

To reveal 1D linear defects by HRTEM, viewing down the longitudinal direction is often required.[51] Unlike 2D planar defects

and 1D linear defects, rotation of the specimen has limited effect on the image contrast patterns of 0D point defects. For example, a spherical inclusion in a crystal would have identical TEM contrast pattern viewed down along any direction.[52] Spherically symmetrical coherency strains resulting from spherical domains lead to a butterfly-like pattern mainly contributed by diffraction contrast. When the spherical domain size reduces, the dark circle image contrast becomes smaller. The smallest point defects in crystals are probably excess atoms in interstitial sites or vacancies at crystal sites. Metal oxides with nonstoichiometric oxygen are in great demand as their ionic conductivity can be improved by controlling the excess oxygen anions or vacancies.[53]

Imaging of point defects by TEM is often very challenging and is not suitable to provide a quantitative measure of the point defect concentration and structure. Firstly, TEM relies on diffraction and interference effect and is therefore not very sensitive to randomly distributed point defects. Frequently, point defects can only be detected by HRTEM when they are in clusters or columns. Secondly, almost all TEM samples are many unit cells thick, and the contrast generated from point defects can often be blocked by the signal from the normal lattice above and below the defect.[54] However, in some special cases, very small point defects, such as random excess oxygen anions, can be detected. Figure 6 (a) shows a typical HRTEM image of $La_4Sr_8Ti_{12}O_{38}$ in a perovskite structure with excess oxygen, with which a high anion conductivity was achieved.[55] Since there is not a large enough space for guest atoms in a perfect perovskite crystal with a formula of ABO_3, the excess oxygen atoms must go to interstitial sites and build up local lattice strain. The resolution of the electron microscope (JEOL JEM-2010) used is not high enough to image randomly located individual oxygen atoms. However, these oxygen atoms would cause local lattice distortion within several atomic layers, leading to a formation of dark spots in the image due to diffraction contrast. The inset of Figure 6 (a) is an enlarged image of one such spot, on which lattice distortion can be seen. As a comparison, Figure 6 (b) shows a HRTEM image of Mg_2SiO_4 nanorod with Co clusters deposited on its surface. Randomly distributed dark spots are also visible but no local lattice distortion is observed.[19] Excess oxygen anions embedded in silicate apatite were also imaged.[56]

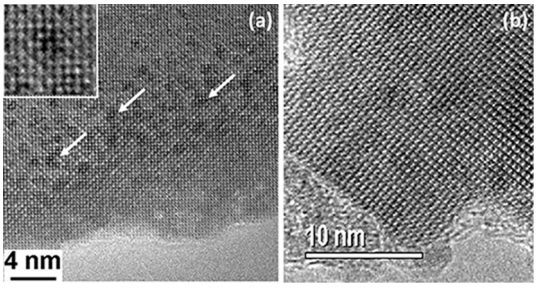

Figure 6. (a) HRTEM image of $La_4Sr_8Ti_{12}O_{38}$, viewing down the [100] zone axis.[55] The arrows indicate some dark spots, which are the locations of excess oxygen anions. The inset shows an enlarged image of a dark spot. (b) HRTEM image of Mg_2SiO_4 nanorod containing Co clusters on its surface.[19] [(a) Reproduced from Ref. 55 with permission from Nature Publishing Group (2006); (b) Reprinted with permission from *J. Phys. Chem. Ser. B* **2004**, *108*, 11561–11566. Copyright (2004) American Chemical Society].

7.3. Disordered Core in Single Crystal Shell

SEM allows us to view particle morphologies. Figure 7(a) shows a SEM image of a perfect icositetrahedral particle of synthetic zeolite analcime. According to the classical theory of crystal growth, the so-called Bravais–Friedel–Donnay–Harker (BFDH) law,[57] crystals exhibit a high symmetric polyhedral shape with facets achieved by different growth rates along different crystal orientations. In other words, the surfaces with the lowest growth rate will be maintained as the final crystals facets. During this "bottom-up" growth process, particles at any stage should be single crystals. However, making a conclusion of a single crystal merely based on the SEM images, e.g. that in Figure 7 (a), is quite risky. In fact, when single crystal XRD was performed on a perfect icositetrahedral particle, the resulted pattern showed a strong polycrystalline ring in addition to some sharp diffraction spots.[58]

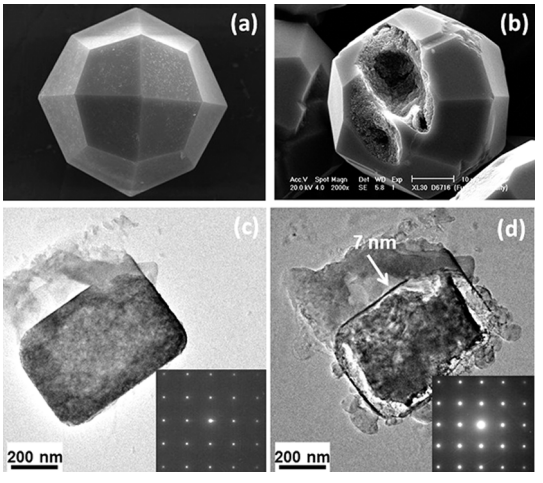

Figure 7. (a) SEM image of an icositetrahedral particle of zeolite analcime. (b) SEM image of a similar icositetrahedron of zeolite analcime with a broken area, showing a polycrystalline core. (c) TEM image of a particle of zeolite A with corresponding SAED pattern. (d) TEM image of the same particle after electron beam irradiation for a few minutes. The inset is the corresponding SAED pattern.[61] [(a,b)Reprinted with permission from *J. Am. Chem. Soc.* **2007**, *129*, 13305–13312. Copyright (2007) American Chemical Society].

When an icositetrahedron is broken, it was observed that the core is polycrystalline, consisting of randomly orientated nanorods of zeolite analcime (Figure 7, b). SEM and TEM investigations of reaction time dependent products revealed that, at an early stage of crystal growth, nanocrystallites of the zeolite did not grow continuously as free crystals in the synthetic solution. Instead, they aggregated into large spherical polycrystalline particles, probably enhanced by the added structure directing agent, ethylamine. The surface of these spherical particles re-crystallised to form a thin icositetrahedral shell. The re-crystallization then extended from the surface to the core of the particles; finally real single crystal polyhedral particles were achieved. A non-classical crystal growth route, i.e. reversed crystal growth, was established based on the electron microscopic observations.[58]

Since then, this phenomenon has been observed in many other materials, including zeolite A, $CaTiO_3$ perovskite, ZnO, CuPt alloy, metal-organic frameworks, and even organic crystals.[59–61]

Figure 7 (c) is a TEM image of a zeolite A particle with the corresponding SAED pattern viewed from the [001] projection. Both the regular shape and the diffraction pattern are normal and indicate a single crystal state. However, under electron beam irradiation for a few minutes, a core-shell structure was detected, i.e. an amorphous core in a very thin single crystal shell (Figure 7, d).[61] Under electron beam exposure, it was seen that the core material appeared more disordered, with a mobile fluid-like appearance and had separated from the thin shell. The almost identical SAED pattern in Figure 7 (d) was actually from the shell of 7 nm in thickness. Consequently, a single crystal type SAED pattern does not always mean the particle under examination is single crystal. On an opposite note, data used to assign $CaCO_3$ mesocrystals, which are a 3D array of iso-oriented single crystal particles are commonly misinterpreted.[18] Roughness on the calcite/polymer crystal surface can be falsely interpreted as homogeneous nanoparticle substructure when in fact, these nanoparticles are only present as a thin surface layer.

SEM/TEM investigations of the non-classical reversed crystal growth allow us to observe many unusual phenomena. For example, HRTEM images show that, at an early stage of the growth of zeolite analcime, the shape of nanocrystallites is plate-like with the short axes along the [111] direction, instead of an icositetrahedron or cube. These nano-crystallites aggregated into some large disks with a perfect self-orientation. Therefore, SAED patterns from these polycrystalline disks are single crystal-like.[58] During the growth of metal organic framework, MOF-5, the first crystalline particles are $Zn_5(OH)_8(NO_3)_2{\cdot}2H_2O$ nanoplatelets with a diameter of 5–10 nm. These nanoplatelets aggregate with the assistance of surface adsorbed 1,4-BDC molecules to form large microplates. $Zn_5(OH)_8(NO_3)_2{\cdot}2H_2O$ underwent a phase transformation to MOF-5. Therefore, in this system, nucleation of MOF-5 crystals does not take place in the solution, but in soft matter aggregates.[60] Because a single crystal shell forms first in a reversed crystal growth route, mass transportation between the particle cores and the outside environment becomes difficult. If the disordered core has a lower density than the crystal, the final crystals would have a hole in the middle. Therefore, the reversed crystal growth mechanism can describe the formation of many hollow crystals.

8. Summary and Outlook

Although HRTEM plays an important role in determination of some complex crystal structures, most researches of electron microscopy, including SEM and TEM, are focussed on microstructures beyond crystal structures, such as crystal size and morphology, crystal facets and growth orientation, local composition and elemental distribution, surface structures and superstructures, and various defects. All of these can be regarded as local structures and the information of these microstructures from XRD and neutron diffraction methods is very limited. However, being deceived by the direct imaging of specimens and their crystal structures, some researchers would simply over-interpret the electron microscopic data. We sometimes see "a real image leads to a wrong conclusion". This article, using some examples, shows how to avoid the over-interpretation of SEM and TEM results. For example, we should not be confused by "particle size" and "crystal size"; extra care should be taken when we try to reveal particle morphology from TEM images; a particle with a perfect polyhedral shape does not mean it must be a single crystal, etc.

Unlike optical microscopy, the formation of image contrast in SEM and TEM is very complicated. For example, in TEM including HRTEM, the formation of image contrast patterns can obey three different principal mechanisms due to different magnification and other microscopic conditions, i.e. mass-thickness contrast, diffraction contrast, and phase contrast. The other electron microscopy related techniques, such as scanning transmission electron microscopic (STEM) imaging, high-angle annular dark-field imaging (HAADF) bring in new elements to the formation mechanisms of image contrast. To correctly understand the images, we must know the principles of these techniques.

Using focused ion beam (FIB) and 3D reconstruction technique, the inner structures of crystals can be easily revealed. Consequently, for studying non-classical crystal growth, more detailed core-shell structures, early stage crystal growth in soft matter aggregates, can be observed. This will help us to understand the non-classical crystal growth, and therefore further control crystal size and morphology.

The state-of-the-art Cs-corrected STEM has a much smaller beam probe and much higher sensitivity to the surface properties of specimens. Detecting nanoscale dipole field and magnetic field in crystalline samples becomes possible. These fields play important roles in crystal growth and self-assembly. Investigation of this is a new direction of electron microscopy. At any stage, it is important to know exactly what we can achieve from the electron microscopic results.

Acknowledgments

W. Z. thanks Professor Jun Yuan for a useful discussion during the revision of this article. The authors wish to thank Engineering and Physical Sciences Research Council (EPSRC) for financial support to the electron microscopy facility (EP/F019580/1) and for a Platform Grant (EP/K015540/1).

Keywords: Electron microscopy · Electron diffraction · Crystal growth · Solid-state structures · Nanostructures

[1] a) Z. Sofer, P. Šimek, O. Jankovský, D. Sedmidubský, P. Beran, M. Pumera, *Nanoscale* **2014**, *6*, 13082–13089; b) C. C. Wilson, *Single Crystal Neutron Diffraction from Molecular Materials*, **2000**, World Scientific, Singapore.
[2] a) L. B. McCusker, C. Baerlocher, *Chem. Commun.* **2009**, 1439–1451; b) F. Gramm, C. Baerlocher, L. B. McCusker, S. J. Warrender, P. A. Wright, B. Han, S. B. Hong, Z. Liu, T. Ohsuna, O. Terasaki, *Nature* **2006**, *444*, 79–81.
[3] X. Zou, S. Hovmöller, P. Oleynikov, *Electron crystallography: electron microscopy and electron diffraction*, *IUCr texts on crystallography*, Oxford University Press, Oxford, **2011**.

[4] a) P. Guo, J. Shin, A. G. Greenaway, J. G. Min, J. Su, H. J. Choi, L. Liu, P. A. Cox, S. B. Hong, P. A. Wright, X. Zou, *Nature* **2015**, *524*, 74–78; b) J. Su, E. Kapaca, L. Liu, V. Georgieva, W. Wan, J. Sun, V. Valtchev, S. Hovmöller, X. Zou, *Microporous Mesoporous Mater.* **2014**, *189*, 115–125.
[5] a) E. Mugnaioli, T. Gorelik, U. Kolb, *Ultramicroscopy* **2009**, *109*, 758–765; b) J. Gjønnes, V. Hansen, A. Kverneland, *Microsc. Microanal.* **2004**, *10*, 16–20.
[6] a) B. D. Forbes, L. Houben, J. Mayer, R. E. Dunin-Borkowski, L. J. Allen, *Ultramicroscopy* **2014**, *147*, 98–105; b) C. Huang, S. Wu, A. M. Sanchez, J. J. P. Peters, R. Beanland, J. S. Ross, P. Rivera, W. Yao, D. H. Cobden, X. Xu, *Nat. Mater.* **2014**, *13*, 1096–1101; c) H. Rösner, C. Kübel, Y. Ivanisenko, L. Kurmanaeva, S. V. Divinski, M. Peterlechner, G. Wilde, *Acta Mater.* **2011**, *59*, 7380–7387.
[7] a) J. M. Thomas, P. A. Midgley, C. Ducati, R. K. Leary, *Prog. Nat. Sci. Mater. Int.* **2013**, *23*, 222–234; b) X. Xie, W. Shen, *Nanoscale* **2009**, *1*, 50–60; c) J. S. Chen, T. Zhu, Q. H. Hu, J. Gao, F. Su, S. Z. Qiao, X. W. Lou, *ACS Appl. Mater. Interfaces* **2010**, *2*, 3628–3635.
[8] a) X. Zhang, J. Qin, Y. Xue, P. Yu, B. Zhang, L. Wang, R. Liu, *Sci. Rep.* **2014**, *4*, 4596; b) J. Zhang, F. Shi, J. Lin, D. Chen, J. Gao, Z. Huang, X. Ding, C. Tang, *Chem. Mater.* **2008**, *20*, 2937–2941; c) P.-C. Lin, S. Lin, P. C. Wang, R. Sridhar, *Biotechnol. Adv.* **2014**, *32*, 711–726.
[9] a) R. Raja, V. B. Golovko, J. M. Thomas, A. Berenguer-Murcia, W. Z. Zhou, S. H. Xie, B. F. G. Johnson, *Chem. Commun.* **2005**, 2026–2028; b) C. Zhang, S. Y. Hwang, Z. Peng, *J. Mater. Chem. A* **2014**, *2*, 19778–19787; c) P. Zhang, Y. Gong, H. Li, Z. Chen, Y. Wang, *Nat. Commun.* **2013**, *4*, 1593–1603; d) Y. Holade, N. E. Sahin, K. Servat, T. W. Napporn, K. B. Kokoh, *Catalysts* **2015**, *5*, 310–348.
[10] W. D. Pyrz, D. J. Buttrey, *Langmuir* **2008**, *24*, 11350–11360.
[11] T. Walther, *J. Microsc.* **2015**, *257*, 171–178.
[12] R. F. Egerton, P. Li, M. Malac, *Micron* **2004**, *35*, 399–409.
[13] a) G. Shi, S. Bao, W. Lai, Z. Rao, X. Zhang, Z. Wang, *Scanning* **2013**, *35*, 69–74; b) J. M. Yuk, M. Jeong, S. Y. Kim, H. K. Seo, J. Kim, J. Y. Lee, *Chem. Commun.* **2013**, *49*, 11479–11481.
[14] a) A. Weibel, R. Bouchet, F. Boulc'h, P. Knauth, *Chem. Mater.* **2005**, *17*, 2378–2385; b) A. Barroso-Bogeat, M. Alexandre-Franco, C. Fernández-González, V. Gómez-Serrano, *J. Microsc.*, **2015**, DOI: 10.1111/jmi.12323.
[15] V. Uvarov, I. Popov, *Mater. Charact.* **2013**, *85*, 111–123.
[16] S. Pabisch, B. Feichtenschlager, G. Kickelbick, H. Peterlik, *Chem. Phys. Lett.* **2012**, *521*, 91–97.
[17] a) T. Ungár, *Scr. Mater.* **2004**, *51*, 777–781; b) B. Pokroy, A. N. Fitch, E. Zolotoyabko, *Adv. Mater.* **2006**, *18*, 2363–2368.
[18] Y.-Y. Kim, A. S. Schenk, J. Ihil, A. N. Kulak, N. B. J. Hetherington, C. C. Tang, W. W. Schmahl, E. Griesshaber, G. Hyett, F. C. Meldrum, *Nat. Commun.* **2014**, *5*, 4341.
[19] S. H. Xie, W. Z. Zhou, Y. Q. Zhu, *J. Phys. Chem. B* **2004**, *108*, 11561–11566.
[20] X. Fu, J. Yuan, *Nanoscale* **2013**, *5*, 9067–9072.
[21] a) X. Xu, Z. Saghi, R. Gay, G. Möbus, *Nanotechnology* **2007**, *18*, 225501; b) I. Florea, C. Feral-Martin, J. Majimel, D. Ihiawakrim, C. Hirlimann, O. Ersen, *Cryst. Growth Des.* **2013**, *13*, 1110–1121; c) L. Cervera Gontard, R. E. Dunin-Borkowski, D. Ozkaya, *J. Microsc.* **2008**, *232*, 248–259.
[22] a) M. C. Scott, C.-C. Chen, M. Mecklenburg, C. Zhu, R. Xu, P. Ercius, U. Dahmen, B. C. Regan, J. Miao, *Nature* **2012**, *483*, 444–448; b) B. Zhang, D. S. Su, *Angew. Chem. Int. Ed.* **2013**, *52*, 8504–8506; *Angew. Chem.* **2013**, *125*, 8662–8664; c) B. Goris, A. De Backer, S. Van Aert, S. Gómez-Graña, L. M. Liz-Marzán, G. Van Tendeloo, S. Bals, *Nano Lett.* **2013**, *13*, 4236–4241.
[23] V. Randle, *J. Microsc.* **1999**, *195*, 226–232.
[24] a) S. A. Fortuna, X. Li, *Semicond. Sci. Technol.* **2010**, *25*, 024005; b) T. R. Kuykendall, M. V. P. Altoe, D. F. Ogletree, S. Aloni, *Nano Lett.* **2014**, *14*, 6767–6773.
[25] Z. Zhang, X. Han, J. Zou, *Sci. China Mater.* **2015**, *58*, 433–440.
[26] a) T. Kuykendall, P. J. Pauzauskie, Y. Zhang, J. Goldberger, D. Sirbuly, J. Denlinger, P. Yang, *Nat. Mater.* **2004**, *3*, 524–528; b) A. H. Chin, T. S. Ahn, H. Li, S. Vaddiraju, C. J. Bardeen, C.-Z. Ning, M. K. Sunkara, *Nano Lett.* **2007**, *7*, 626–631.
[27] S. Ristig, O. Prymak, K. Loza, M. Gocyla, W. Meyer-Zaika, M. Heggen, D. Raabe, M. Epple, *J. Mater. Chem. B* **2015**, *3*, 4654–4662.
[28] a) L. Gan, M. Heggen, S. Rudi, P. Strasser, *Nano Lett.* **2012**, *12*, 5423–5430; b) J.-H. Lee, J.-T. Jang, J.-S. Choi, S. H. Moon, S.-H. Noh, J.-W. Kim, J.-G. Kim, I.-S. Kim, K. I. Park, J. Cheon, *Nat. Nanotechnol.* **2011**, *6*, 418–422.
[29] W. Z. Zhou, D. A. Jefferson, J. M. Thomas, *Proc. Roy. Soc. Lond. Ser. A* **1986**, *406*, 173–182.
[30] R. Johnson, *Energy dispersive X-ray microanalysis*, Noran Instruments, Middleton, Wisconsin, **1999**.
[31] F. Mou, L. Xu, H. Ma, J. Guan, D.-R. Chen, S. Wang, *Nanoscale* **2012**, *4*, 4650–5657.
[32] D. Tzoulaki, L. Heinke, M. Castro, P. Cubillas, M. W. Anderson, W. Z. Zhou, P. A. Wright, J. Kärger, *J. Am. Chem. Soc.* **2010**, *132*, 11665–11670.
[33] J. Park, M. D. Porter, M. C. Granger, *Langmuir* **2015**, *31*, 3537–3545.
[34] G. Kothleitner, M. J. Neish, N. R. Lugg, S. D. Findlay, W. Grogger, F. Hofer, L. J. Allen, *Phys. Rev. Lett.* **2014**, *112*, 085501.
[35] a) F. Maier-Flaig, C. Kübel, J. Rinck, T. Bocksrocker, T. Scherer, R. Prang, A. K. Powell, G. A. Ozin, U. Lemmer, *Nano Lett.* **2013**, *13*, 3539–3545; b) L. Han, U. Wiedwald, J. Biskupek, K. Fauth, U. Kaiser, P. Ziemann, *Beilstein J. Nanotechnol.* **2011**, *2*, 473–485; c) Y. C. Bae, A. R. Lee, G. H. Baek, J. B. Chung, T. Y. Kim, J. G. Park, J. P. Hong, *Sci. Rep.* **2015**, *5*, 13362.
[36] A. N. Chiaramonti, L. D. Marks, *J. Mater. Res.* **2005**, *20*, 1619–1627.
[37] a) P.-X. Gao, P. Shimpi, H. Gao, C. Liu, Y. Guo, W. Cai, K.-T. Liao, G. Wrobel, Z. Zhang, Z. Ren, H.-J. Lin, *Int. J. Mol. Sci.* **2012**, *13*, 7393–7423; b) X. Zou, H. Fan, Y. Tian, S. Yan, *CrystEngComm* **2014**, *16*, 1149–1156; c) X. Huang, M.-G. Willinger, H. Fan, Z.-L. Xie, L. Wang, A. Klein-Hoffmann, F. Girgsdies, C.-S. Lee, X.-M. Meng, *Nanoscale* **2014**, *6*, 8787–8795.
[38] W. Z. Zhou, D. A. Jefferson, W. Y. Liang, *Surf. Sci.* **1989**, *209*, 444–454.
[39] a) C. Lai, Q. Wu, J. Chen, L. Wen, S. Ren, *Nanotechnology* **2010**, *21*, 215602; b) F. Li, P. D. Nellist, D. J. H. Cockayne, *Appl. Phys. Lett.* **2009**, *94*, 263111.
[40] W. Z. Zhou, A. Asab, I. Gameson, D. A. Jefferson, P. P. Edwards, *Phys. C* **1995**, *248*,1–10.
[41] W. Z. Zhou, D. A. Jefferson, W. Y. Liang, *J. Solid State Chem.* **1992**, *98*, 437–441.
[42] W. Z. Zhou, J. M. Thomas, *Curr. Opin. Solid State Mater. Sci.* **2001**, *5*, 75–83.
[43] N. Nassif, N. Pinna, N. Gehrke, M. Antonietti, C. Jäger, H. Cölfen, *Proc. Natl. Acad. Sci. USA* **2005**, *102*, 12653–12655.
[44] V. Pecharsky, P. Zavalij, *Fundamentals of powder diffraction and structural characterisation of materials*, Springer, New York, **2009**.
[45] Y. S. Meng, G. Ceder, C. P. Grey, W.-S. Yoon, Y. Shao-Horn, *Electrochem. Solid-State Lett.* **2004**, *7*, A155–A158.
[46] a) W. Z. Zhou, *J. Solid State Chem.* **1992**, *101*, 1–17; b) W. Z. Zhou, D. A. Jefferson, J. M. Thomas, *J. Solid State Chem.* **1987**, *70*, 129–136; c) W. Z. Zhou, *J. Solid State Chem.* **1988**, *76*, 290–300.
[47] W. Z. Zhou, *J. Solid State Chem.* **2002**, *163*, 479–483.
[48] a) U. Wiedwald, L. Han, J. Biskupek, U. Kaiser, P. Ziemann, *Beilstein J. Nanotechnol.* **2010**, *1*, 24–47; b) F. Meng, M. Estruga, A. Forticaux, S. A. Morin, Q. Wu, Z. Hu, S. Jin, *ACS Nano* **2013**, *7*, 11369–11378; c) H. Shi, B. Dong, W. Wang, *Nanoscale* **2012**, *4*, 6389–6392; d) J. C. Meyer, C. Kisielowski, R. Erni, M. D. Rossell, M. F. Crommie, A. Zettl, *Nano Lett.* **2008**, *8*, 3582–3586; e) K. P. McKenna, F. Hofer, D. Gilks, V. K. Lazarov, C. Chen, Z. Wang, Y. Ikuhara, *Nat. Commun.* **2014**, *5*, 5740–5747; f) M. I. den Hertog, C. Cayron, P. Gentile, F. Dhalluin, F. Oehler, T. Baron, J. L. Rouviere, *Nanotechnology* **2012**, *23*, 025701.
[49] A. C. McLaughlin, W. Z. Zhou, J. P. Attfield, A. N. Fitch, J. L. Tallon, *Phys. Rev. B* **1999**, *60*, 7512–7516.
[50] Z. X. Su, C. Dickinson, Y. T. Wan, Z. L. Wang, Y. W. Wang, J. Sha, W. Z. Zhou, *CrystEngComm* **2010**, *12*, 2793–2798.
[51] P. A. Wright, W. Z. Zhou, J. Pérez-Pariente, M. Arranz, *J. Am. Chem. Soc.* **2005**, *127*, 494–495.
[52] M. F. Ashby, L. M. Brown, *Philos. Mag.* **1963**, *8*, 1649–1676.
[53] G. Wang, Y. Ling, Y. Li, *Nanoscale* **2012**, *4*, 6682–6691.
[54] a) C. A. Geiger, *Solid solutions in silicate and oxide systems*, Eötvös University Press, Budapest, Hungary, **2001**; b) G. Van Tendeloo, D. Van Dyke, S. J. Pennycook, *Handbook of nanoscopy*, Wiley-VCH, Weinheim, Germany, **2012**.
[55] J. C. Ruiz-Morales, J. Canales-Vázquez, C. Savaniu, D. Marrero-López, W. Z. Zhou, J. T. S. Irvine, *Nature* **2006**, *439*, 568–571.
[56] Y. Q. Zhang, Z. X. Su, A. K. Azad, W. Z. Zhou, J. T. S. Irvine, *Adv. Energy Mater.* **2012**, *2*, 316–321.
[57] a) A. Bravais, in: *Études Crystallographic*, Gauthier-Villars, Paris, **1866**; b) M. G. Friedel, *Bull. Soc. Fr. Mineral. Cristallogr.* **1907**, *30*, 326–455; c) J. D. H.

Donnay, D. Harker, *Am. Mineral.* **1937**, *22*, 446–467; d) P. Hartman, W. G. Perdok, *Acta Crystallogr.* **1955**, *8*, 521–524.

[58] X. Y. Chen, M. H. Qiao, S. H. Xie, K. N. Fan, W. Z. Zhou, H. Y. He, *J. Am. Chem. Soc.* **2007**, *129*, 13305–13312.

[59] a) X. F. Yang, J. X. Fu, C. J. Jin, J. Chen, C. L. Liang, M. M. Wu, W. Z. Zhou, *J. Am. Chem. Soc.* **2010**, *132*, 14279–14287; b) K. Self, H. J. Zhou, H. F. Greer, Z. R. Tian, W. Z. Zhou, *Chem. Commun.* **2013**, *49*, 5411–5413; c) F. J. Yu, W. Z. Zhou, *Prog. Nat. Sci. Mater. Int.* **2013**, *23*, 331–337; d) J. R. G. Sander, D.-K. Bučar, J. Baltrusaitis, L. R. MacGillivray, *J. Am. Chem. Soc.* **2012**, *134*, 6900–6903; e) K. Self, M. Telfer, H. F. Greer, W. Z. Zhou, *Chem. Eur. J.* **2015**, *21*, 19090–19095.

[60] C. M. Zheng, H. F. Greer, C.-Y. Chiang, W. Z. Zhou, *CrystEngComm* **2014**, *16*, 1064–1070.

[61] J. F. Yao, D. Li, X. Y. Zhang, C. H. Kong, W. B. Yue, W. Z. Zhou, H. T. Wang, *Angew. Chem. Int. Ed.* **2008**, *47*, 8397–8399; *Angew. Chem.* **2008**, *120*, 8525–8527.

Received: November 18, 2015
Published Online: ■

Electron Microscopy

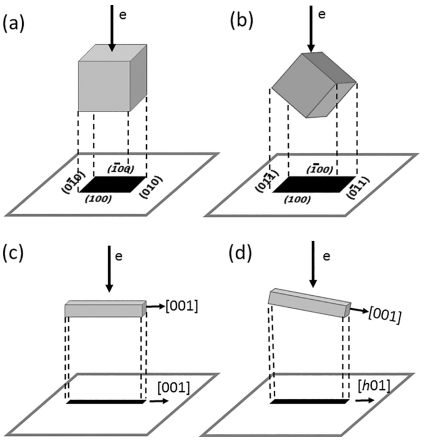

Some examples of conventional SEM and TEM studies of inorganic crystals are reviewed. Typical problems of misinterpretation of the images are discussed.

DOI: 10.1002/ejic.201501342